Research Journal of Pharmaceutical, Biological and Chemical Sciences

Synthesis, Characterization and Electrical Properties of Zr doped ZnO Nanoparticles and its Effect on Photodegradation of Methyl Orange.

Adly A Hanna, Walied A A Mohamed*, Hoda R Galal, and Ammar A Labib.

Inorganic Chemistry Department, National Research Center, Cairo, Egypt.

ABSTRACT

Pure nano-sized zinc oxide and doped with zirconium were prepared by using sol-gel route. Different percentages of Zr were doped through the preparation process. The produced samples were characterized using x-ray diffraction and the particle size was calculated by scherrer's equation. Also the morphology of the samples were performed by using SEM techniques. The results of measurements revealed that the obtained particles are nano-size particles ranging from 28 to 54 nm, also the lattice parameters a and c were calculated. It is found that as the percentage of Zr increases the bond length increases from 1.98 to 2.00 ^{o}A due to the segregation of ZnO through the structure and the resistivity decreases from 0.343 to 0.050, also the band gap decreases slightly from 3.388 to 3.280 ev. The photodegradation percentage of methyl orange in presence of ZnO doped with Zr reached to 90% and behaves as a first order.
Keywords: doped ZnO, Nano zinc oxide, ZrO_2, resistivity, energy gap and photodegradation rate.

*Corresponding author

INTRODUCTION

Transition metal oxides such as Zn, Sn, Zr, Ti and etc… have been found different technological applications due to their semiconducting properties [1]. Different modifications were carried to improve their structure and the electrical properties to increase their application in the advanced techniques such as solar energy [2], sensors devices [3] and biomedical applications [4]. This modification includes two processes; the first one is the modification of the particle size [5] and another is doping host cations which lead to change the structure and the morphology of the doped oxides.

The preparation of nano-sized transition metal oxide introduced additive properties which create new applications to these oxides. Among the nano structured transition metal oxides, special attention was paid to Zn and Zr oxides owing to their unique feature and different methods of applications. The literature survey shows that ZnO in an n-type semiconductors with excellent properties where it have a wide energy gap, a large excitant binding energy at room temperature and it is chemically and thermal stable during the reaction time [6-8]. Both the electrical and the optical properties of ZnO changes greatly by doping with other cations. This change in the properties of ZnO was related to the nature of dopant cation as well as the preparation method route [9-12]. Different methods were used to the preparation of metal doped ZnO nano particles such as the solid-solid reaction, co-precipitation [13], hydrothermal [14, 15] and sol–gel methods [16]. Sol–gel process was considered as one of a preferable method because it gives a homogenous product. In this work Zr doped ZnO was prepared by using sol–gel process to obtain nano-particle products. The prepared doped ZnO was characterized by using the spectroscopic and the morphology techniques. Also, the aim of this work extend to apply the produced nano-particle in the photodegradation of methyl orange as a waste material through the dyeing process in the textile factories.

It is noteworthy that about 10%–15% of the dyes used in different industries fields are lost in the effluents during the dying process [17]. In general, this dye is considered as one of common dyes as an environmental pollutant in wastewater in many different industrials field. There are many trials were done to remove this dye from wastewater [18]. Photocatalytic process is a more suitable for the removal of dyes [19-22] than the conventional treatment techniques. In this work, the photodegradation of methyl orange MO can be effectively enhanced by using zinc oxide doped zirconium oxide.

MATERIAL AND METHODS

Materials

Zirconium Nitrate $Zn(NO_3)_2.4H_2O$, Zirconium Oxy Chloride $ZrOCl_2$ and Citric acid $(C_6H_8O_7).H_2O$ supplied from SIGMA-ALDRICH and Methyl Orange (Sodium 4-[(4-dimethylamino) phenyldiazenyl] benzenesulfonate $(C_{14}H_{14}N_3NaO_3S)$), M. wt. 327.33 was purchased from SIGMA-ALDRICH, ACS reagent, dye content 85%. All chemicals used in this work were of analytical grade reagents without any further purification.

Synthesis of Zr doped ZnO nanoparticles

Synthesis of nanocrystalline powder samples of Zr doped ZnO (0.2 %, 0.4 %, 0.6 % and 0.8 %) have been prepared through sol-gel-combustion method using $Zn(NO_3)_2.4H_2O$, $ZrOCl_2$ and citric acid as starting materials. The constituents, in the desired proportion, were dissolved in distilled water and carefully mixed in a 100 ml beaker to obtain a 50 ml aqueous solution, which then stirred for about 3 h at 110 ^{0}C and then it was evaporated under constant stirring. Water was completely evaporated then the solution converted in the form of gel. This gel was subsequently converted into foam phase and after a strong self-propagating combustion reaction at 210 ^{0}C gives a fine powder. This fine powder was ground for 45 min and annealed at 500 ^{0}C for 3 h followed by repeat grounding for 1 h and sintering at 700 ^{0}C for 3 h.

Characterization of Zr doped ZnO particles

X-ray diffraction (XRD)

X-ray diffraction (XRD) (X0 Pert MPD, Ni filtered Cu-Kα_radiation, Phillips) was used for the identification of nanocrystalline powder samples of Zr doped ZnO particles (λγ = 1.5418 A^0), operated at

voltage of 30 kV and current of 15 mA, in 2ϑ range from 10^0 to 100^0 with scan rate of 2^0/min and a step size of 0.02^0. Debye Scherrer formula has been used to determine the crystallite size of the samples [18].

The morphology of the samples

The surface morphology of Zr doped ZnO particles were characterized by scanning electron microscopy (SEM) (JEOL-JSM 5800LV, Japan).

Electrical measurements

The electrical parameters were measurement by HIOKI 3532-50 LCR HITESTER (RS-232C), Japan.

Photoactivity instrument

The experimental set up was employed for the photocatalytic studies by using photoreactor 500-W Hg-lamp (Eng. Co., Ltd., Egypt). The concentration of MO dye solution was $2 \times 10{-}5M$. The concentration of MO dye after photodegradation was analysed by using a UV-V is spectrophotometer (Schmdazo) by measuring the change in absorbance values at 464 nm.

RESULTS AND DISCUSSION

XRD of Zr doped ZnO particles

The XRD patterns of pure and different Zr doped ZnO particles samples (0, 0.2 %, 0.4%, 0.6 % and 0.8 %) are shown in Fig. 1. The structural parameters and phase purity have been studied using the powder X-ray diffraction, the diffraction patterns of all samples can be indexed to the hexagonal wurtzite structure of ZnO using the standard data (JCPDS-36-1451) [19], and no trace of Zr related phase were found. Thus, there is no change in the wurtzite structure by the addition of Zr ion into the ZnO matrix indicating that the Zr dopant to incorporate into the lattice as substitutional ion [20].

The crystallite size (γ) for different samples were calculated by using the Debye–Scherrer's formula [23]:

$$\gamma = \frac{\kappa\lambda}{B\cos\theta} \qquad (1)$$

Where k is the X-ray wavelength, B is full width at half maximum in radians, K is the shape factor and θ is the Bragg angle. The results indicate that the particle size of pure ZnO equal to 22 nm and its value increase gradually by doping with zr cation to reach 54 nm at Zr=0.8%. In all cases, the prepared samples lies in the nano-particle crystals. On other hand the values of the lattice parameters a and c were calculated for the doped and undoped samples. It is found that the lattice parameters increase slightly from 3.2475–3.2501 ^{o}A and from 5.2042–5.2075 ^{o}A for a and c parameters respectively. This findings means that as ZnO doped with Zr, the lattice parameters expanded as shown in Table 1. The expansion may due to the change in radius of Zr and Zn, where it equal to 0.80 Å and 0.74Å for Zn. Fig. 3 shows a slight shift of (002) and (101) peaks towards the smaller angle with an increase in Zr content corresponding to linear increment in the lattice parameters a and c accordance to Vegard's law. This increment of lattice parameters also, may be attributed to the ionic radius of Zr^{4+} (84) which is larger than that of Zn^{2+}(74) [24, 25]. The difference in the ionic radius for Zr and Zn cause a slight expansion in the bond length where it changes from 1.9817 to 2.0024 ^{o}A at 0.8% of Zr. As the content of Zr increases in ZnO the more Zn^{2+} are substituted by Zr^{4+}, the greater the lattice distortion of ZnO would be generated causing the more lattice expansion. So these results indicate that the Zn ions are well substituted by Zr ions and forming a single phase compound. The Zn–O bond lengths (ι) for all Zr doped and undoped samples are calculated according to the following equations, [26].

$$l = \sqrt{\left(\frac{a^2}{3} + \left(\frac{1}{2} - u\right)^2 c^2\right)} \qquad (2)$$

where the positional parameter u in the wurtzite structure is given by

$$u = \frac{a^2}{3c^2} + 0.25 \qquad\qquad (3)$$

And the calculated value is tabulated in Table 1. It has been observed that with the increase in Zr content into the structure the bond length increases and this may be due to the segregation of ZnO [27].
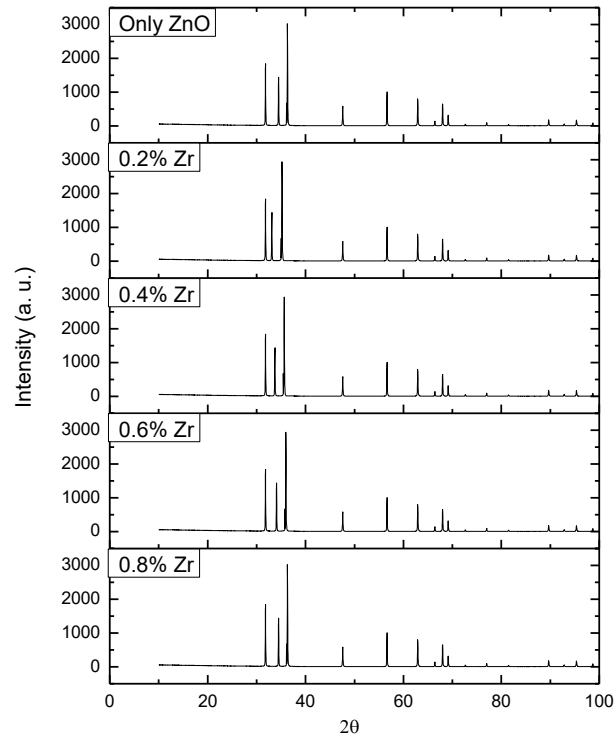

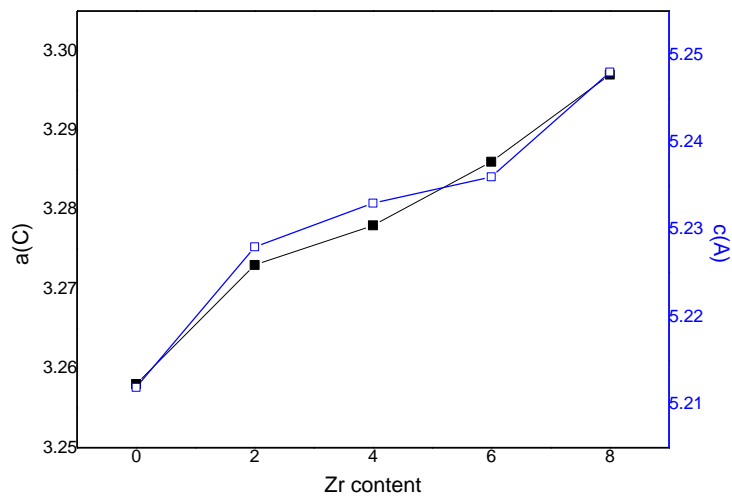**Fig. 1 X-ray patterns of nano zinc oxide and its doped samples with Zr content**

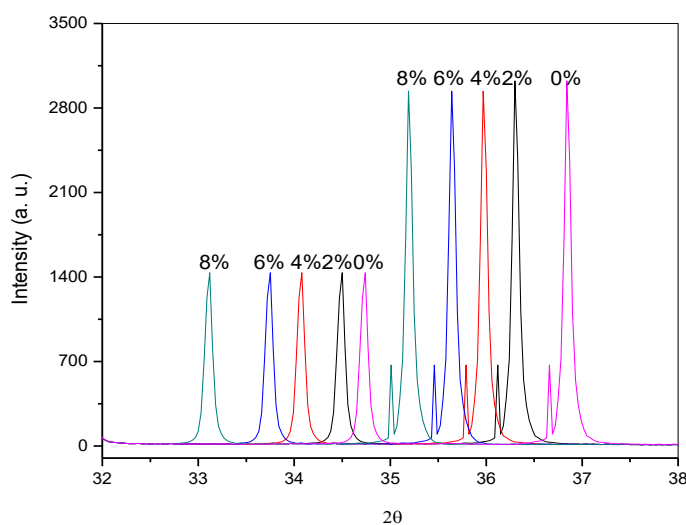**Fig. 2 Variation of lattice parameters (a and c) with Zr content.**

Fig. 3 X-ray patterns shift for doping of Zr on nano zinc oxide peak at (2θ = 34.74   and 36.84)

Table 1: The calculated lattice parameters, particle size and bond length of the doped ZnO

Zr conc. %	Particle Size (nm)	Lattice parameters		c / a	Zn-O bond length *l* (Å)
		a (Å)	c (Å)		
0	22	3.258	5.211	1.599	1.9817
0.2	28	3.273	5.228	1.597	1.9900
0.4	35	3.278	5.233	1.596	1.9927
0.6	44	3.286	5.236	1.593	1.9964
0.8	54	3.297	5.248	1.591	2.0024

Scanning electron microscopy (SEM)

SEM images of different doped amount of Zr are shown in Figs. 4-7. The micrographs of the samples indicate that the surface morphology of Zr doped ZnO particles are in nanoparticles scale, which are not entirely in spherical shape and the surface is not much smooth pattern. So it seems that the nanoparticles are almost uniform in size while some particles are hexagonal shape (Figs.(4,5)) at.0.2% and 0.4% doped samples go to be become small in the crystallite size and the surface is not much smooth. On further doping (Fig. 6, 7) at.0.6% and 0.8%, larger crystals break onto smaller size and the surface becomes smoother again.

The analysis of the SEM micrographs shows that as ZnO doped with 0.2 and 0.4% Zr show that the crystalline size is small (Figs. 4 and 5), while as the percentage of doping increases to 0.6 and 0.8%, the larger crystals are exhibited and these crystals are brown and the surface become smooth.
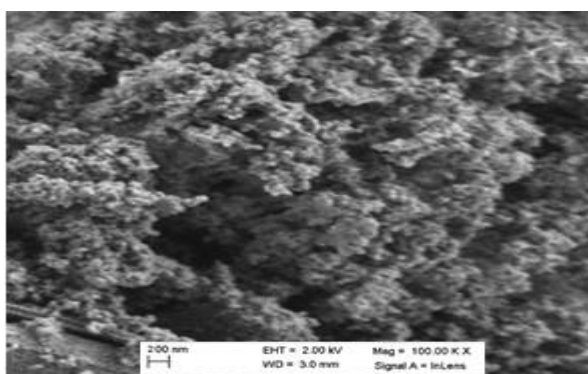

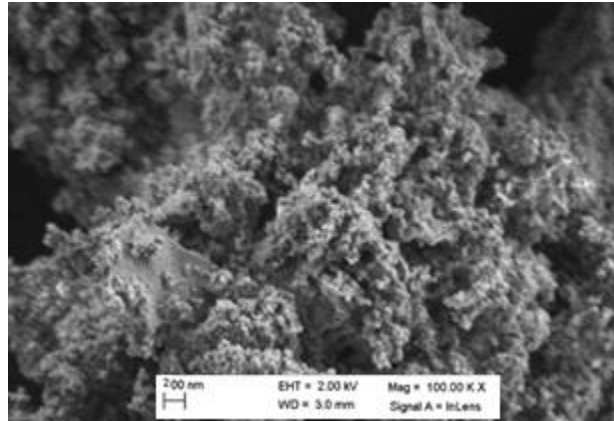**Fig. 4 SEM of nano ZnO doped with 0.2% Zr**
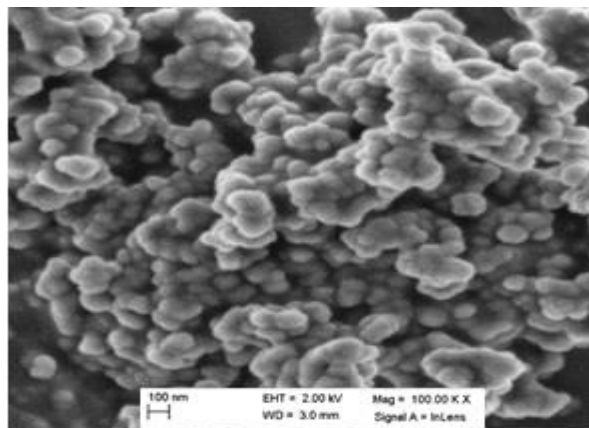
Fig. 5 SEM of nano ZnO doped with 0.4% Zr

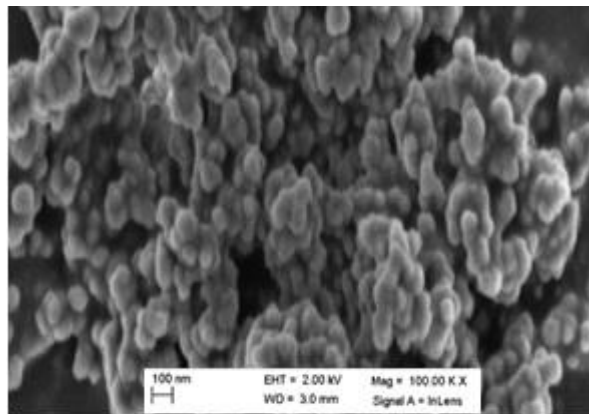**Fig. 6 SEM of nano ZnO doped with 0.6% Zr**

Fig. 7 SEM of nano ZnO doped with 0.8% Zr

Electrical measurements

The AC resistivity of the doped and undoped samples were measured at room temperature (Table 2). The values of the resistivity were recorded in Table 2. The results of measuring show that it equal to 0.343 for the pure nano zinc oxide and it decreases to become equals 0.050. It is noteworthy, that the values of resistivity decreases rapidly till ZnO doped with 0.4% Zr and it converted to less decrease between 0.4 % and 0.8 % Fig. 8. This findings may be explained by considering that Zr atom acts as n-type dopant that is presumed to replace Zn atoms, hence increasing the free electron density (N_d) by increasing Zr content. This replacements seen to be great at low dopant atoms and dispersed at high doping concentration. From the resistivity measurements both the carrier concentrate and mobility of ions were calculated. The results show

that the carrier concentrate increases from 2.2 to 23.7 as the content of zirconium increases Fig. 9. The mobility is related to the scattering frequency v and the effective mass m_e^* through

$$\mu H \frac{e}{vm_e^*} \qquad (4)$$

Where e is the electronic charge. The results of calculation Fig. 10. Show that the mobility decreases rapidly till 0.2 % Zr was doped, while it decreases slightly between 0.2 % - 0.8 % Zr.

Table 2: The resistivity, carrier conc., mobility and band gap of the doped ZnO with Zr

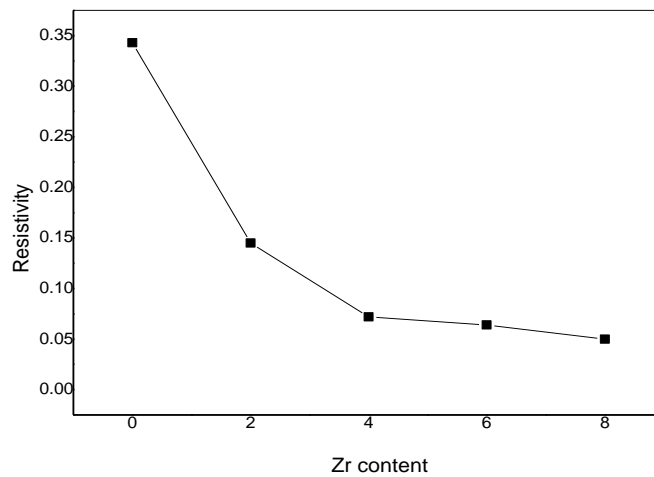| Zr conc. %	Resistivity ρ (Ω cm)	Carrier conc., $N_d \times 10^{18}$ (cm^{-3})	Mobility μ (cm^2 V^{-1} S^{-1})	Band gap E_g (ev)
0	0.343	2.2	14.5	3.388
0.2	0.145	9.6	9	3.363
0.4	0.072	14.4	8.1	3.328
0.6	0.064	19.8	7.1	3.299
0.8	0.050	23.7	6.6	3.280

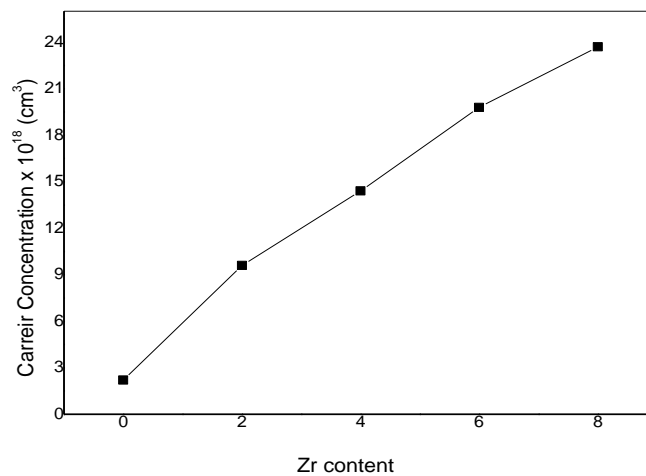**Fig. 8 Variation of resistivity with Zr content**

Fig. 9 Variation of carrier concentration with Zr content.
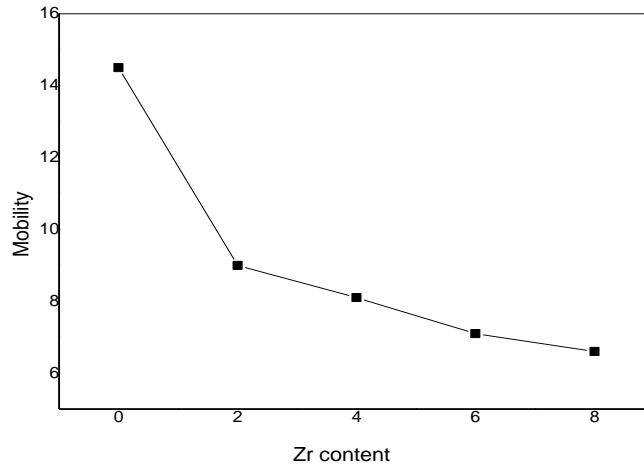
Fig. 10 Variation of mobility with Zr content

Optical band gap

The band gap is one of main optical properties of semiconducting nanoparticles for expectation of absorbance value. There are another several factors such as oxygen deficiency, size and structure of nanoparticles, surface roughness and impurity centers [28]. The optical band gap was evaluated using the Tauc relation [29].

$$\alpha h v = K \left(h v - E_g \right)^n \qquad (5)$$

Where a is the absorption coefficient (α = 2.303 *A/t*, A is the absorbance and *t* is the thickness of the cuvette), K is a constant, hv is the photon energy and E_g is the optical energy band gap and the value of n = 1/2, 1, 3/2 and 2 and it depends on the nature of the transition. The value of n = 1/2 is considered for direct band gap semiconductor. The optical band gap decreases with doping concentration increases as shown in the Fig. 11. This decrease in the band gap may be due to increasing of the lattice parameters (31).
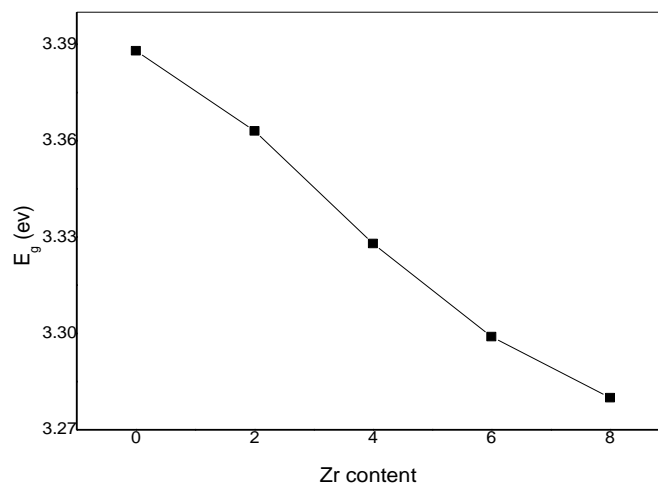

Fig. 11 Variation of optical band gap with Zr content

Photoactivity

The photoactivity is one of the most recently advanced technologies used in the decomposition of textile dyes to minimize the pollutions. In this study for example the photodegradation of Methyl Orange MO

was followed over a period of 160 min Fig. 12. The results Show that degradation occurs following the adsorption of UV-Vis radiation and over a 160 min period nearly more than 90% of the compound could be removed at different doped amount of different Zr doped ZnO particles samples. However, in half the time nearly more than 60% of the compound could be removed. The Langmuir-Hinshelwood model was used to determine the photocatalytic performance of the dye using the equation:

$$\ln(C_o/C) = kt \qquad (5)$$

Where *Co/C* is the normalized MO concentration, *t* is the reaction time, and *k* is the apparent reaction rate constant. Fig. 12 depicts the kinetics of MO degradation by plotting the normalized concentration with time. The results indicate that the doped amount of different Zr doped ZnO particles samples showed increases in photodegradation efficiency with increasing of doping concentration.
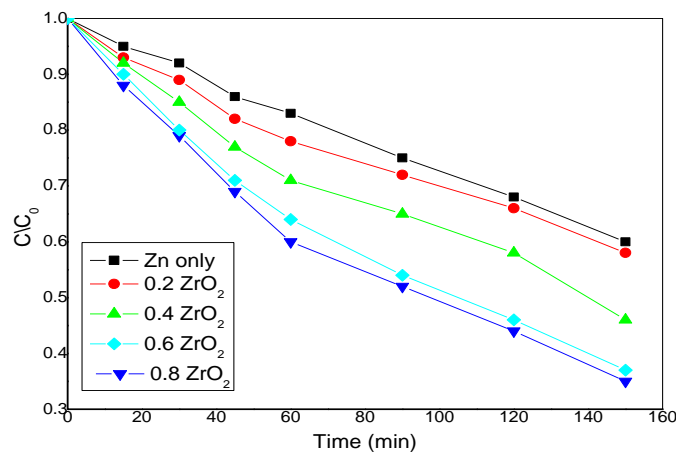

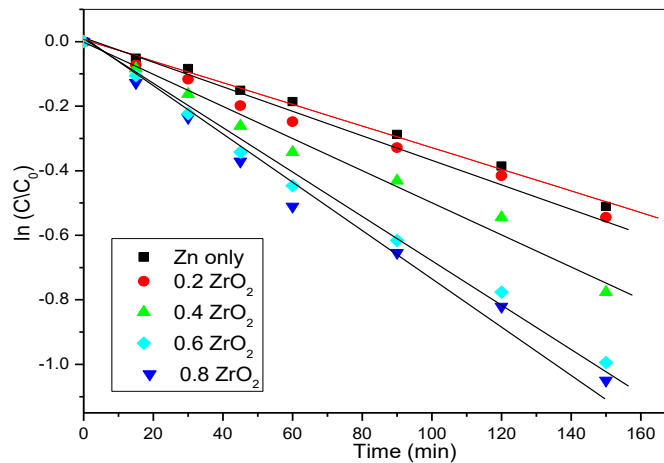**Fig. 12 Normalized concentration of pfotodegradation of methyl orange with different Zr content**

Fig. 13 kinetic reaction rates for pfotodegradation of methyl orange with different Zr content

Table 3: Photodegradation rates

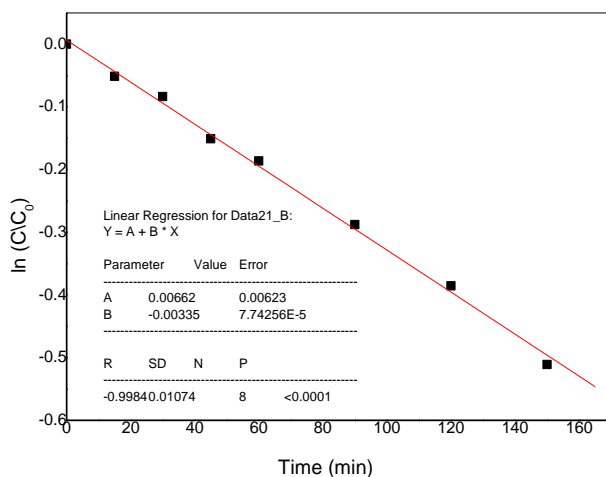| Doping Oxide	Rate (Min^{-1})
Zn only	33.5×10^{-2}
0.2% Zr	34.8×10^{-2}
0.4% Zr	48.4×10^{-2}
0.6% Zr	64.9×10^{-2}
0.8% Zr	68.2×10^{-2}

Fig. kinetic reaction rates for pfotodegradation of methyl orange without Zr content
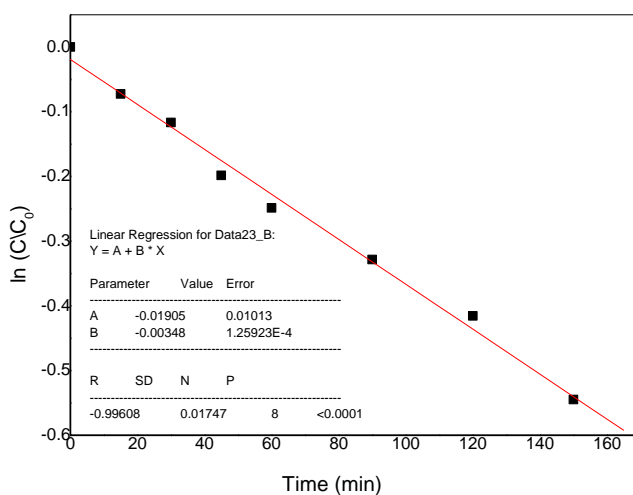

Fig. kinetic reaction rates for pfotodegradation of methyl orange with 0.2 % Zr content
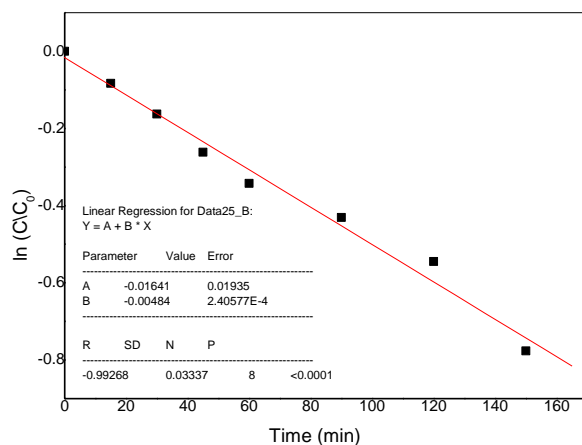

Fig. kinetic reaction rates for pfotodegradation of methyl orange with 0.4 % Zr content
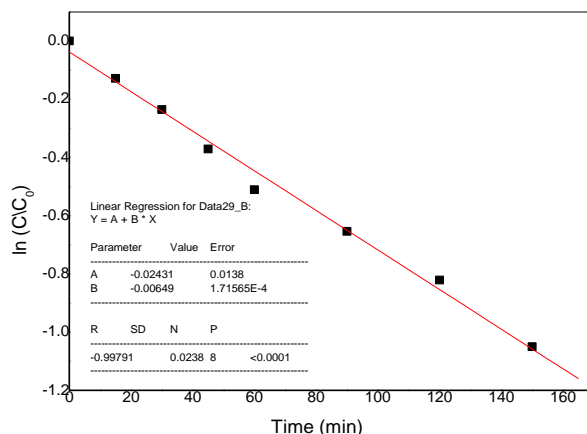
Fig. kinetic reaction rates for pfotodegradation of methyl orange with 0.6 % Zr content
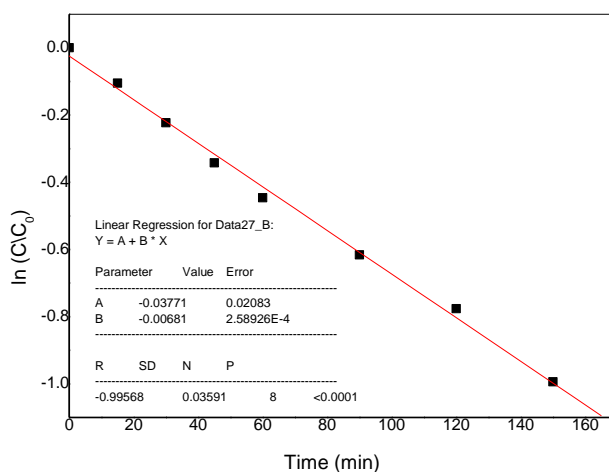

Fig. kinetic reaction rates for pfotodegradation of methyl orange with 0.8 % Zr content

CONCLUSION

The replacing of some Zn ions with Zr one improvement the semiconducting properties of ZnO according to the analysis for observed measurements. Also the electrical resistivity of the doped samples decreases with Zr content, while the carrier concentrate increases and the mobility decreases. The application of the doped ZnO with Zr on the photodegradation of methyl orange shows that 90 % of the pollutant dyes removed after 160 min by using doped Zr as agents.

REFERENCES

[1]. Imran Khan, Shakeel Khan , Razia Nongjai, Hilal Ahmed, Wasi Kh. Optical Materials 35 (2013) 1189–1193
[2]. Liu Z, Liu C, Ya J, Lei E. Renew. Energy 2011; 36: 1177-1181.
[3]. Meng F, Yin J, Duan Y Q, Yuan Z H, Bie L. J. Sensor Actuator B 2011; 156: 703-708.
[4]. Ghule K, Ghule A V, Chen B J, Ling Y C. Green Chem. 2006; 8: 1034-1041.
[5]. Adli A Hanna, Walied A A Mohamed, Hoda R Galal. Egyptian journal of chemistry 2014; 57, 5,6: 343-352.
[6]. Stefanic G, Grzeta B, Popovic S, Music S. Croat. Chem. Acta 1999; 72: 395.
[7]. Stefanic G, Stefanic I Mater. Chem. Phys. 2000; 65: 197-207.
[8]. Su S C, Bell A T. J. Phys. Chem. B 1998; 102: 7000-7007.
[9]. Minami T. Semicond. Sci. Technol. 2005; 20: S35-S44.
[10]. Bhat S V, Deepak F L. Solid State Commun. 2005; 135: 345-347.

[11]. Deka S, Joy P A. Solid State Commun. 2007; 142: 190-194.
[12]. Jing C, Jiang Y, Bai W, Chu J, Liu A. J. Magn. Magn. Mater. 2010; 322: 2395-2400.
[13]. Meng F, Yin J, Duan Y Q, Yuan Z H, Bie L. J. Sensor Actuator B 156 (2011) 703.
[14]. Yogamalar N R, Bose A C. J. Solid State Chem. 2011; 184: 12-20.
[15]. Sahoo T, Kim M, Baek J H, Jeon S R, Kim J S, Yu Y T, Lee C R, Lee I. H. Mater. Res. Bull. 46 (2011) 525.
[16]. Liu H, Yang J, Hua Z, Zhang Y, Yang L, Xiao L, Xie Z. Appl. Surf. Sci. 2010; 256: 4162-4165.
[17]. Murugesan K, Dhamija A, Nam I H, Kim Y M, Chang Y S. Dyes Pigments 2007; 75: 176-184.
[18]. Yuanjie Su, Yang Ya, Hulin Zhang, Yannan Xie, Zhiming Wu, Yadong Jiang, Naoki Fukata, Yoshio Bando, Zhong Lin Wang. Nanotechnology 24 (2013) 295401.
[19]. Wang Y J, Lu K C, Feng C G. J. Rare Earths 2013; 31: 360-365.
[20]. Wu J, Zhang G L, Liu J, Gao H B, Song C X, Du H R, Zhang L, Gong Z P, Lü Y G. J. Rare Earths 2014; 32: 727.
[21]. Wang Z L. Adv. Mater. 2011; 24: 280–285.
[22]. Agorku E S, Kuvarega A T, Mamba B B, Pandey A C, Mishra A K. J. Rare Earths Vol. 33, No. 5, May 2015, P. 498
[23]. Waren B E, X-ray Diffraction, Addison-Wesley, Reading, MA, 1969.
[24]. Mezdrogina M M, Danilevskii E Y, Kuz'min R V, Poletaev N K, Trapeznikova I N, Chukichev M V, Bordovskii G A, Marchenko A V, Eremenko M V. Semiconductors 44 (2010) 426.
[25]. Fornasiero P, Monte R D, Rao G R, Kaspar J, Meriani S, Trovaralli A, Graziani M. J. Catal. 151 (1995) 168.
[26]. Srinivasan G, Rajendra Kumar R T, Kumar J. J. Sol–Gel Sci. Technol. 43 (2007) 171–177.
[27]. Signal S, Kaur J, Namgyal T, Sharma R. Physica B 407 (2012) 1223.
[28]. Ahmed A S, Shafeeq M M, Singla M L, Tabassum S, Naqvi A H, Azam A. J. Lumin. 131 (2010) 1.
[29]. Tauc J, Amorphous and Liquid Semiconductors, Plenum Press, New York, 1974. p. 171.
[30]. Joshi G P, Saxena N S, Mangal R, Mishra A, Sharma T P. Bull. Mater. Sci. Indian Acad. Sci. 26 (2003) 387.